Bull. Chem. Soc. Ethiop. **2008**, 22(2), 225-236. ISSN 1011-3924
Printed in Ethiopia

THE STRUCTURE OF NIOBIUM-DOPED $MoSe_2$ AND WSe_2

Moussa Bougouma[1], Boubié Guel[1,*], Tiriana Segato[2], Jean B. Legma[1] and Marie-Paule Delplancke Ogletree[2]

[1]Laboratoire de Chimie-Physique et d'Electrochimie, UFR/SEA, Université de Ouagadougou 03 BP 7021 Ouagadougou 03, Burkina Faso
[2]Service Matières et Matériaux, Groupe Chimie Industrielle, Faculté des Sciences Appliquées, Université Libre de Bruxelles CP 165/63, Avenue F.D.Roosevelt 50 B-1050 Bruxelles, Belgique

(Received June 22, 2007; revised October 22, 2007)

ABSTRACT. Polycrystalline niobium-doped molybdenum and tungsten diselenides were synthesized in silica tubes sealed under secondary vacuum. They were characterized by scanning electron microscopy, electron diffraction, X-ray diffraction, chemical composition and EDX analyses. The morphology of niobium-doped molybdenum solid solutions was shown to depend strongly on the conditions of synthesis, whereas the structural characterization did not.

KEY WORDS: Polycrystalline niobium-doped molybdenum and tungsten diselenide solid solutions, Doped powders diselenides, $Mo_{1-x}Nb_xSe_2$, $W_{1-x}Nb_xSe_2$, SEM, X-ray diffraction, Electron diffraction

INTRODUCTION

Molybdenum diselenide ($MoSe_2$) and tungsten diselenide (WSe_2) are transition metal semiconducting dichalocogenides, which crystallize in the 2H-MoS_2 structures. The $2H_b$-polytype of these MSe_2 (M = Mo, W) layer compounds consists of three planes: one hexagonal plane consisting of the metal ions M, placed between two hexagonal planes consisting of the Se ions [1]. The sequence of the planes in these layers is **…**Se−M−Se Se−M−Se**…**. Within each layer, the coordination of M is trigonal prismatic and the bonding is strongly covalent. The layers are held together by weak van der Waals forces and at the interface of the MSe_2 units a set of octahedral and tetrahedral vacant sites is created. These sites are available to be occupied by a variety of foreign atoms, ions or neutral molecules to form new phases [2, 3]. The $2H_b$-polytype contains two Se–M–Se sheets. $MoSe_2$ also crystallizes in the 3R structure, which contains three sheets and the coordination of the metal atoms is again trigonal prismatic.

$MoSe_2$ and WSe_2 have been the subject of many investigations since they were shown to have potential applications in solar energy conversion by Tributsch and Gerischer [4-6]. Their band gap width is between 1 and 2 eV [7], so a great part of the solar spectrum can be used to excite $d \rightarrow d$ transitions. If they are used as semiconducting electrodes in a photo galvanic cell, electrode corrosion is avoided, as the bonding electrons are not affected by the excitation process. Solar-to-electrical conversion efficiencies in the range of 17% to 20 %, greater than those of single crystal silicon, could be achieved for MSe_2 electrodes in a polyiodide electrolyte [8].

In previous work [9] we examined ways to increase the photoconductivity of MSe_2 transition metal n-type dichalcogenides. Niobium- and rhenium-doped single crystals were obtained by chemical vapour transport from a polycrystalline 1 % metal-doped solid solution, using as transport agent iodine in the case of $MoSe_2$, and $SeCl_4$ in the case of WSe_2 [Throughout this

*Corresponding author. E-mail: boubie.guel@univ-ouaga.bf

paper % composition denotes atomic %]. For a $Mo_{1-x}Re_xSe_2$ phase with $x \approx 6 \times 10^{-5}$, the photocurrent gain was increased by a factor of 10 without any applied voltage and the electrical conductivity was at its maximum. The best saturation current (550 A m^{-2}) was obtained for $Mo_{1-x}Nb_xSe_2$ $x \approx 1 \times 10^{-4}$. This value was the highest ever found in the literature for transition metal dichalcogenides. However, no detailed study was carried out on the polycrystalline metal-doped solid solution to understand why the insertion of niobium into the network of MSe_2 creates deep donor levels, which then enhance the n-type character of the resulting single crystals.

Many experiments on WSe_2 single crystals have shown that the electronic properties of the materials depend strongly on the synthesis conditions of the polycrystalline powder used for the crystal growth [10]. Deviations from stoichiometry could be related to packing defects, dislocations, polytype variations and inhomogeneity of dopant concentration in the initial polycrystalline powder. It was, for example, shown that molybdenum diselenides with a ratio Se/Mo < 1.9 were characterized by a mixed-stacking of the $2H_b$-and 3R-type layers. The existence of both interstitial Mo and Se vacancies in the $MoSe_2$ lattice was also suggested for materials with $1.9 \leq Se/Mo \leq 2.0$ [11]. Analysis of the nature of the polycrystalline charge, prior to its use in the halogen transport process, seem to be very important for further understanding of the single crystal growth process.

In the present study, polycrystalline powders $M_{1-x}Nb_xSe_2$ with x = 0, 1 and 5 % were characterized by X-ray diffraction and microanalysis. The morphology of the powders was also investigated by scanning electron microscopy and transmission electron microscopy. The effects of the doping material Nb on the lattice parameters are discussed.

EXPERIMENTAL

Synthesis of MSe_2 and doped powder diselenides $M_{1-x}Nb_xSe_2$

The syntheses were in silica glass tubes sealed under secondary vacuum (10^{-6} Torr or $13.32.10^{-5}$ Pa). For the synthesis of molybdenum and tungsten diselenides, the ampoule contained a mixture of molybdenum or tungsten powder, Koch-Light, 99.9% pure; and granular selenium, Koch-Light, 99.999% pure. For doped powder synthesis, a measured mass of the doping material (elemental niobium, 99.9% pure, Koch-Light) was added to the appropriate mixture.

Two types of procedures were then followed. In the first, the samples were heated to 600 °C over 48 h in steps to avoid explosions due to sudden selenium vaporization. They were kept at this temperature for up to 72 h, and then air-quenched. After fine milling, the samples were annealed at 1000 °C for 96 to 120 h, and slowly cooled in the furnace to room temperature. In the second procedure, the samples were heated to 750 °C over 48 h in steps and kept at this temperature for up to 120 h; then slowly cooled to room temperature. After fine milling, the samples were annealed at 1050 °C for up to 168 h, then slowly cooled in the furnace to room temperature. We shall refer to powders prepared by the two procedures as A type and B type, respectively.

Characterization of polycrystalline powders

The structural parameters of the polycrystalline powders were determined by X-ray powder diffraction (XRD) using a nickel-filtered Cu-Kα radiation (λ = 1.5406 Å) in a Siemens D5000 apparatus (Brüker), and the computer programs Diffrac Plus and Topaz V2.0. The XRD data were recorded in the 2θ-range 10-70° at a scan speed of 0.08° min^{-1}. Lattice parameters were refined using a least-squares technique.

Scanning electron microscopy (SEM JEOL JSM-6100) and transmission electron microscopy (TEM Philips CM 20) were used for the morphological characterization of the powders.

The Se/Mo ratios of the samples $MoSe_2$ and WSe_2 were analyzed by a gravimetric procedure [11, 12]. The samples were oxidized in air at 973 K and 1023 K for 12 h giving MoO_3 and WO_3 respectively. The metal M (M = Mo, W) content of the samples was determined from the mass of MO_3 formed. The Se content was then estimated by subtraction of the metal mass from the initial mass of the sample.

RESULTS AND DISCUSSION

Since the properties of the single crystals are strongly dependent of the polycrystalline charge used in the halogen transport process, it is of interest to compare the morphology and the structure of the two types of samples (A and B samples). It is also of interest to compare metal-doped and undoped materials to explore the influence of the dopant Nb on the morphology and the structure of MSe_2 polycrystalline powder.

Undoped molybdenum and tungsten diselenides powders

Under the experimental conditions described above, the surfaces of the materials showed a lamellar structure with a metallic luster. Individual hexagonal plates can be clearly distinguished.

For Type A (Figure 1a) and B (Figure 1b) $MoSe_2$ powders, we have well-developed crystals. The crystals sizes range from 50 to 100 μm wide with a thickness of 5-10 μm (A type $MoSe_2$) and from 15 to 47 μm wide with a thickness of 2-8 μm (B type $MoSe_2$). A type $MoSe_2$ contains a few crystals whose size even reaches 200 μm. The luster is brighter for A type than for B type crystals. A type powders show crystals whose surfaces contain defects that could be potential sites for crystallization. In contrast, B type $MoSe_2$ powders exhibit crystals with smoother surfaces.

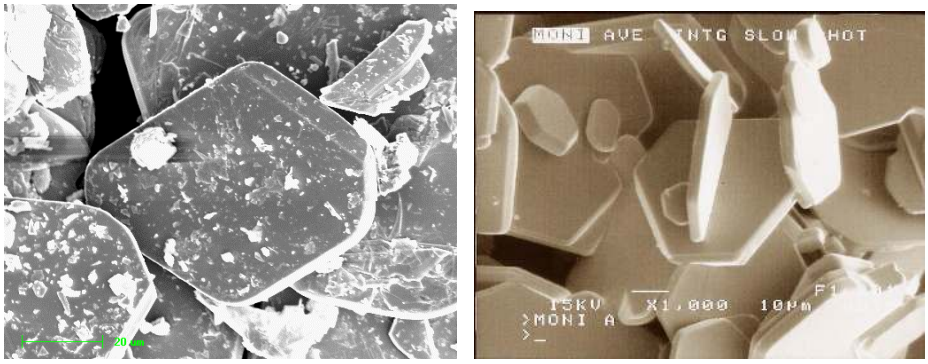

(a) (b)

Figure 1. Scanning electron microscopic images of molybdenum diselenide: (a): A type molybdenum diselenide polycrystalline powder (13 mm = 20 μm) and (b): B type molybdenum diselenide polyscristalline powder (6 mm = 10 μm).

Typical XRD patterns for A type and the B type $MoSe_2$ powders are shown in Figure 2. For A type $MoSe_2$, the most intense peaks observed, due to a preferred orientation of the plate-shaped crystals, are from basal plane reflections: (002), (006), (008). Weaker (004), (103) and (105) peaks are also observed. The (100), (102), (104) and (106) peaks are also visible in the A type $MoSe_2$ XRD pattern, though with much smaller intensities. The B type $MoSe_2$ XRD pattern does not indicate a preferred orientation of the (00*l*) basal planes, since intense diffraction peaks from the (002), (100), (103), (105) planes are observed, the most intense peak being the (103) reflection. All diffraction angles in patterns in Figure 2 are in agreement with the literature values for hexagonal $MoSe_2$ [13]. The refined lattice parameters are listed in Table 1. In the X-ray diffraction pattern of B type $MoSe_2$, the widths of (103) and (105) peaks are broader than those of the (002) and (100) peaks whereas all the diffraction lines of A type $MoSe_2$ are narrow. The results of chemical composition analysis are listed in Table 2. These results indicate that the composition is stoichiometric for A type MSe_2 powders (M = Mo, W).

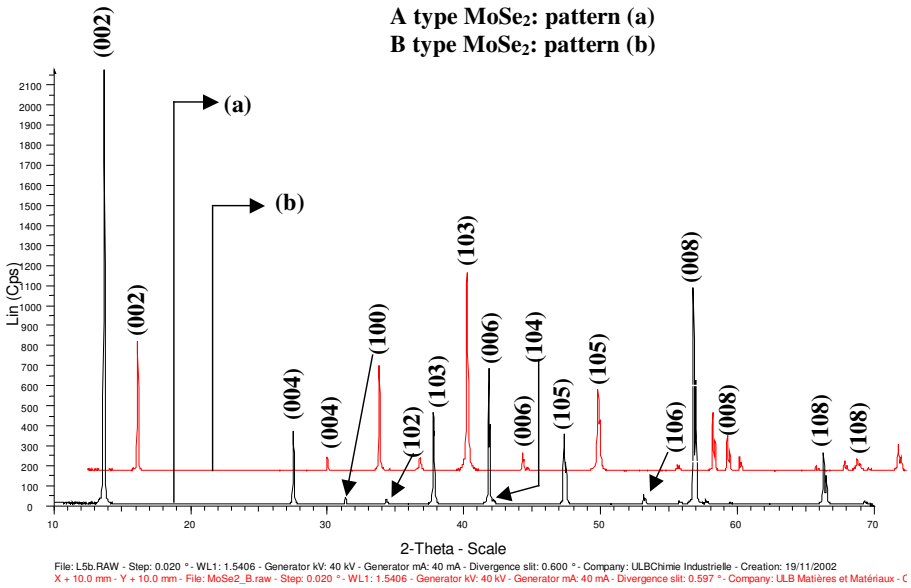

Figure 2. X-ray diffraction patterns of A and B types molybdenum diselenide polycrystalline powder: (a) A type $MoSe_2$: scale (X, Y), (b) B type $MoSe_2$: scale (X + 10.0 mm, Y + 10.0 mm).

The morphologies of A and B types WSe_2 powders are similar to those of the corresponding A and B types $MoSe_2$ powders, except that in B type WSe_2, the thickness ranges from 2 to 4 μm. Typical XRD patterns are shown in Figure 3 for A and B type WSe_2 powders. In both patterns, intense diffraction peaks from the (002), (006), (008), (100), (103) and (105) planes are observed. All diffraction lines are narrow and 2θ values are in agreement with the literature data for hexagonal WSe_2 [14]. The refined lattice parameters and the Se/W ratios are listed in Table 1 and Table 2, respectively.

In the system Mo-Se three phases seem to be well established, i.e. Mo_3Se_4, $MoSe_2$ and $MoSe_3$, and at present only two polytypes of $MoSe_2$ are known, namely the $2H_b$-and 3R-types [11]. These polytypes are the same that are found for the disulfide MoS_2. A unit cell of $2H_b$-type $MoSe_2$ contains two Se-Mo-Se sheets, whereas that of 3R-type contains three sheets.

Table 1. Lattice parameters* for undoped and Nb-doped MSe_2 (M = Mo, W) powders.

Material	Parameters		
	a (Å)	*c* (Å)	*c*/*a*
WSe_2[a], A	3.2864(7)	12.9817(0)	3.9500(4)
1% Nb-doped WSe_2[a], A	3.2879(5)	12.9698(7)	3.9446(7)
WSe_2[a], B	3.2871(2)	12.9844(8)	3.9501(0)
1% Nb-doped WSe_2[a], B	3.2887(9)	12.9792(6)	3.9465(1)
5 % Nb-WSe_2[a], B	3.2947(7)	12.9400(8)	3.9274(6)
WSe_2[b]	3.2860(0)	12.9800(0)	3.9500(9)
$MoSe_2$[a], A	3.2906(0)	12.9369(9)	3.9315(0)
1% Nb-doped $MoSe_2$[a], A	3.2916(4)	12.9131(8)	3.9230(2)
$MoSe_2$[a], B	3.2905(9)	12.9352(5)	3.9309(8)
1% Nb-doped $MoSe_2$[a], B	3.2920(6)	12.9249(2)	3.9260(9)
5% Nb-$MoSe_2$[a], B	3.3004(3)	12.8587(3)	3.8960(8)
$MoSe_2$[c]	3.2890(0)	12.9270(0)	3.9303(7)

*Lattice parameters are given with an experimental error of ±0.0001 Å. [a]This work; A = A type powder; B = B type powder. [b]JCPDS n° 87-2418. [c]JCPDS n° 77-1715. Some of the calculated values contain zeros that could be considered as significant figures because they do not locate the decimal point. These zeros do not match the standard deviation because they can not be read directly and with certainty from a scale or instrument read out. They are only the results of numerical calculations.

Table 2. Results of Se/M (M = Mo, W) ratios for undoped $MoSe_2$ and WSe_2 powders*.

Material	Analysed Se/M (M = Mo, W)
$MoSe_2$, A	2.0255
WSe_2, A	2.0255
$MoSe_2$, B	1.8857
WSe_2, B	1.9148

*Each ratio Se/M is given with an error of ±0.0003. The ratio Se/M has been calculated from experimental gravimetric measurements, using an electronic analytical balance ($\Delta m = 0.0001$ g).

According to Naruko *et al.* [11], the non-stoichiometric range for $MoSe_2$ polycrystalline powder is estimated to be $1.85 \leq Se/Mo \leq 2.0$. The homogeneous range has been divided into two parts: $1.85 \leq Se/Mo < 1.9$ and $1.9 \leq Se/Mo \leq 2.0$. It has been shown that for the composition range $1.85 \leq Se/Mo < 1.9$, the peak widths of (10*l*) family are significantly larger and this has been attributed to a mixed-stacking of the $2H_b$ and 3R-type layers [11]. This is a well-known feature for hexagonal close-packed crystals having a stacking disorder: the (00*l*) and (*hk*0) peaks are narrow, but the (*h*0*l*) peaks are usually broad [14].

Our results show the same effect: for B type $MoSe_2$, the (00*l*) and (*hkl*) peaks are narrow, whereas the (*h*0*l*) peaks are broad. Moreover, the Se/Mo ratio is found within experimental errors to be within the range $1.85 \leq Se/Mo < 1.9$. It is thus suggested that B type $MoSe_2$ powder exhibits a mixed-layer structure in agreement with the literature. In contrast, all the diffraction lines of the A type $MoSe_2$ powder are sharp, indicating a genuine $2H_b$ structure with a Se/Mo ratio in the composition range $1.9 \leq Se/Mo \leq 2.0$, within experimental errors. The structure of the diselenide WSe_2 is similar to the disulfide WS_2, with the metal trigonally prismatically surrounded by selenium [3]. But unlike WS_2, the only known modification of WSe_2 is the 2H-type and no rhombohedral diselenide has been found.

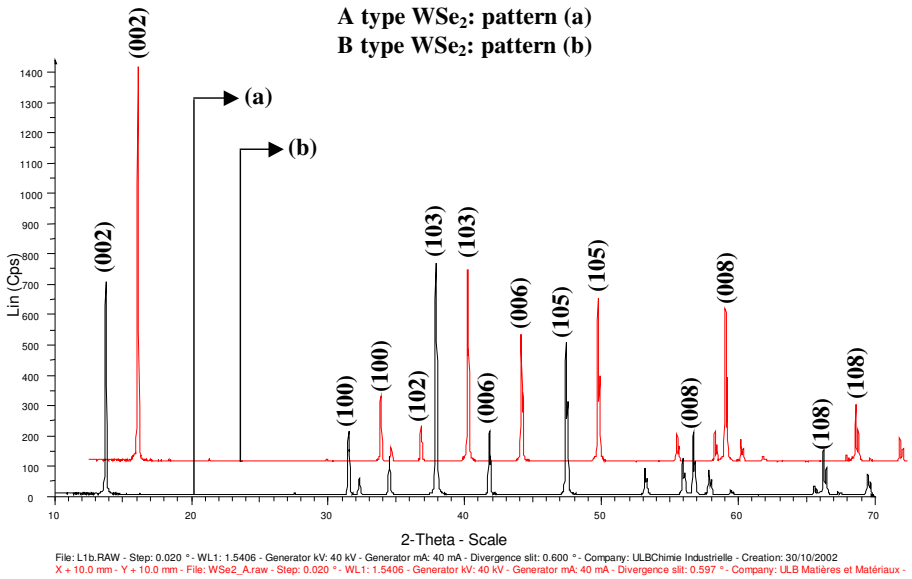

Figure 3. X-ray diffraction patterns of A and B types tungsten diselenide polycrystalline powder: (a) A type WSe_2: scale (X, Y), (b) B type WSe_2: scale (X + 10.0 mm, Y + 10.0 mm).

Doped powders of diselenides: $M_{1-x}Nb_xSe_2$ (M = Mo, W)

Doped powders of diselenides $Mo_{1-x}Nb_xSe_2$

For polycrystalline niobium-doped $MoSe_2$ materials, no great differences were observed between the SEM images of A type 1 % Nb-doped $MoSe_2$ and the A type undoped $MoSe_2$ samples. Both showed the same morphological features. Although the A type 1 % niobium-doped $MoSe_2$ crystallizes with the same structure as the A type $MoSe_2$ sample (Figure 4 and Table 1), from Table 1 we notice that in the presence of increasing amounts of Nb *a* increases and *c* decreases. All diffraction lines in the XRD pattern of the A type 1 % Nb-doped $MoSe_2$ sample are narrow. Very intense diffraction peaks from (002), (103), (105), (008) and also relatively intense diffraction peaks from (004), (100), (006) are observed in the diagram (Figure 4b). Figure 4b shows a very small peak at $2\theta \approx 29.70°$, which has not been assigned.

The case of the B type 1 % Nb-doped $MoSe_2$ sample is more complex. The SEM images (Figure 5) show two categories of particles: large and small. Large particles of these compounds show the same features as those that have already been described for the B type undoped $MoSe_2$ sample. Figure 5a depicting a B type 1 % Nb-doped $MoSe_2$ sample shows a characteristic example of these large particles, which are well-developed hexagonal crystals. Small particles of the B type 1 % Nb-doped $MoSe_2$ sample are shown in Figures 5b. The main difference between the large and small particles is that the small ones do not have a hexagonal shape, but they generally form blocks with rectangular cross-section and length ranging from 5 to 9 µm. At larger magnifications a box shows alternate dark and bright nested fringes with a mean distance of 1 µm. The dark fringes appear hollower than the bright ones. These small particles appear to be sintered together and dispersed among the larger plate-like crystallites. The results of composition analysis performed by electron probe microanalysis in a TEM, on both the large and small particles are given in Table 3. There is no evidence for the presence of any foreign

elements. The non-stoichiometry of the large particles is demonstrated by the experimental ratio Se/Mo equal to 1.67, i.e. we have a non-stoichiometric phase, which could be formulated as $Mo_{0.96}Nb_{0.03}Se_{1.67}$, with a deficiency of Se and an excess of both Mo and Nb compared with the composition $Mo_{0.99}Nb_{0.01}Se_2$ of the 1 % Nb-doped solid $MoSe_2$. With a large excess of Mo, composition of the small particles is far from a metal-doped $MoSe_2$ composition. To get more information on the structures of the large and small particles, electron diffraction (THEED) patterns were obtained. The THEED pattern obtained on the large particles is given in Figure 6a. It indicates a distorted hexagonal close-packed layered structure. In contrast, the THEED pattern for the small particles (Figure 6b) does not correlate with a hexagonal close-packed layered structure.

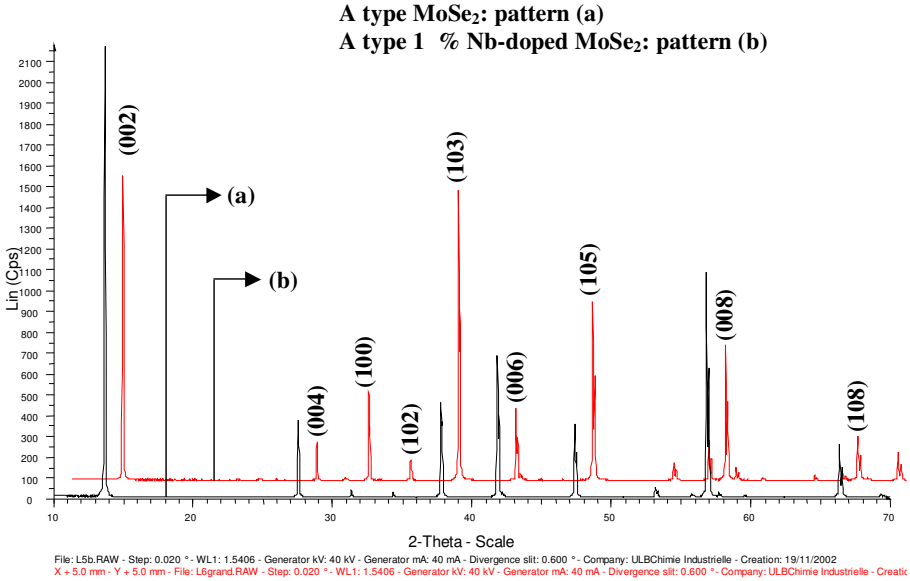

Figure 4. Comparison of X-ray diffraction patterns of: (a) A type $MoSe_2$: scale (X, Y), (b) A type 1 % niobium-doped $MoSe_2$: scale (X + 5.0 mm, Y + 5.0 mm).

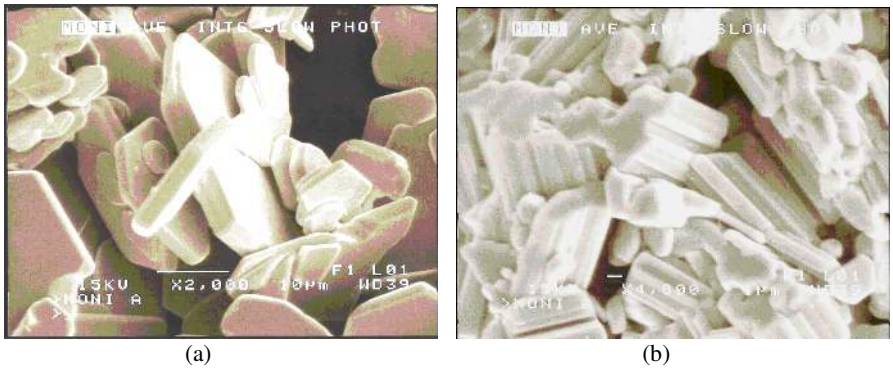

(a) (b)

Figure 5. Scanning electron microscopic images of B type niobium-doped $MoSe_2$ polycrystalline powder: (a) large particles of Nb-doped $MoSe_2$ (12 mm = 10 µm), (b) small particles of Nb-doped $MoSe_2$at larger magnification (3 mm = 1 µm).

Table 3. Results of the chemical analysis of particles in a B type Nb-doped $MoSe_2$ powder.

Element	Weight	Atomic %
Large particles		
SeK	57.1	61.8
NbK	1.3	1.1
MoK	41.6	37.1
Total	100.0	100.0
Small particles		
SeK	2.1	2.5
NbK	3.6	3.7
MoK	94.3	93.8
Total	100.0	100.0

The XRD pattern corresponding to the B type 1 % Nb-doped $MoSe_2$ sample is shown in Figure 7b. The same intense diffraction lines as those described for the type B undoped $MoSe_2$ sample are observed here. The diffraction lines from the B type 1 % solid solution are broader than those from their undoped counterpart. To verify that this characteristic was a consequence of the synthetic procedure the B type 5 % Nb-doped $MoSe_2$ sample was synthesized. As expected, the XRD pattern (Figure 7c) confirms that the diffraction lines broaden with increasing concentration of niobium. This broadening is not limited to those reflections (h-k = $3n \pm 1$; n = 0 or integer) normally attributed to stacking faults in these materials [15-17], it is suggested that the broadening indicates some inhomogeneous distribution of niobium within the B type sample [17]. The B type 5 % Nb-doped $MoSe_2$ sample is formed as large and small particles with the same features as those of the 1 % Nb-doped counterpart. The small Mo-rich particles are not detected in the XRD-patterns of the 1 and 5 % Nb-doped $MoSe_2$. Despite their crystallinity, their concentration is most probably below the detection limit. The lattice parameters for both B type doped $MoSe_2$ samples are listed in Table 1. As previously described for the A type 1 % Nb-doped $MoSe_2$ sample, a increases, while c decreases for the large particles of the B type 1 % and 5 % Nb-doped $MoSe_2$ samples.

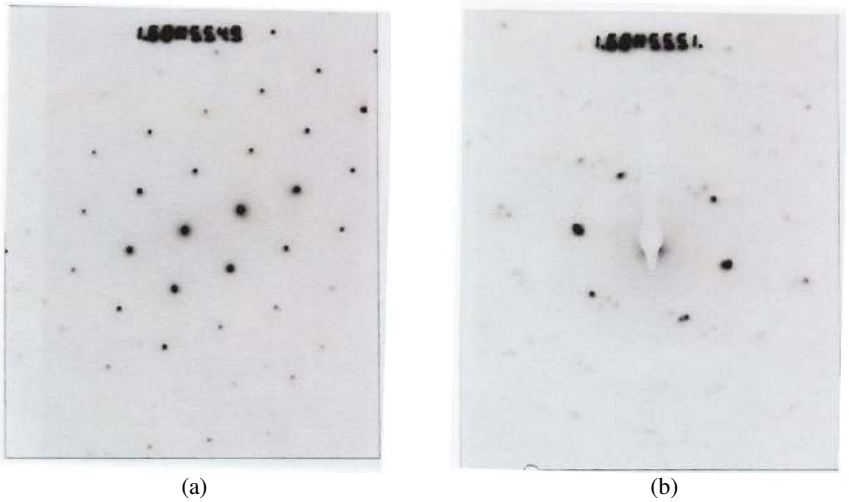

(a) (b)

Figure 6. (a) THEED pattern of large particles in a B type 1 % Nb-doped $MoSe_2$ polycrystalline powder. (b) THEED pattern of small particles in a B type 1 % Nb-doped $MoSe_2$ polycrystalline powder.

The crystallite size for $x = 0, 0.01, 0.05$ was calculated using the Scherrer's formula [3]:

$$t = (k\lambda)/(\beta \cos \theta_0) \quad (1)$$

where t is the crystallite thickness as measured perpendicular to the reflecting plane, k is the Scherrer's constant whose value is chosen as unity assuming the particle to be spherical, λ is the wavelength of the X-ray radiation, β is the width at half-intensity in radians, and θ_0 is the Bragg angle. The crystallite sizes for $x = 0, 0.01, 0.05$ are listed in Table 4. The values have a precision of 10 nm but there is clearly a gradual decrease in the size with increasing niobium content. This suggests that there is an increase in the number of defects.

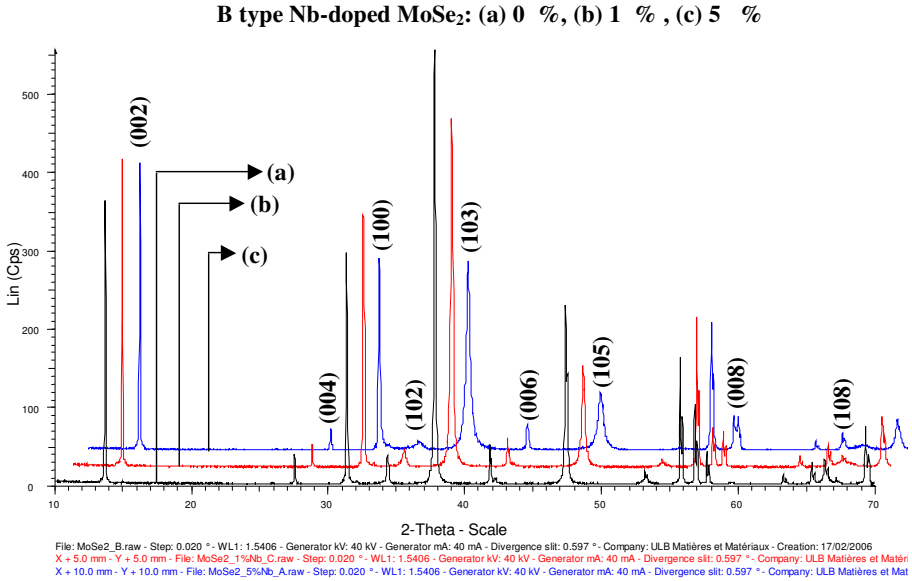

Figure 7. Comparison of X-ray diffraction patterns of B type $MoSe_2$ polycrystalline powders: (a) $MoSe_2$: scale (X, Y), (b) 1 % Nb-doped $MoSe_2$: scale (X + 5.0 mm, Y + 5.0 mm), (c) 5 % Nb-doped $MoSe_2$: scale (X + 10.0 mm, Y + 10.0 mm).

Table 4. Particle sizes (nm) found for B type Mse_2 (M = Mo, W; $x = 0, 0.01, 0.05$) polycrystalline powders.

hkl	Material		
	1 % Nb-doped WSe_2	5 % Nb-doped WSe_2[a]	WSe_2
002	116	113	126
103	119	113	152
006	103	116	180
105	112	117	167
008	129	105	211
	1 % Nb-doped $MoSe_2$	5 % Nb-doped $MoSe_2$	$MoSe_2$
002	127	127	145
103	86	32	117
006	113	90	173
105	90	25	118
008	112	87	210

Analysis of the doping of $M_{1-x}Nb_xSe_2$ solid solutions shows that the effects of introduction of niobium into these dichalcogenides can be very complex. There are two possible ways of inserting metallic ions into the layered dichalcogenides structures [18].

(1) A metal ion can intercalate between two layers, in view of the weak van der Waals forces, which link them together. This well known process involves a distorsion of the crystal and/or a variation of the Fermi level. The sandwiched metal ions create stronger bonds than the original van der Waals forces and convert the two-dimensional structure of the compound into a three-dimensional structure. It has been shown that molybdenum diselenides can intercalate Group III-A elements, Ga, In and Tl, forming non-stoichiometric compounds [19]. Ga^{3+}, In^{3+} and Tl^{+} ions have been shown to diffuse into the interlayer space of $MoSe_2$, where they occupy positions in trigonal-prismatic environments. This leads to an increase in the lattice constant *c*, from that of molybdenum diselenide, the lattice constant *a* being unchanged [19]. It has also been shown that intercalation of indium in WSe_2 does not produce any change in *a* whereas there was an increase in *c* with increasing amounts of indium [3].

(2) A metal ion can be substituted for a M atom in a MSe_2 layer (M = Mo, W) without any structural change. It has been shown that in the $Ti_{1-x}Nb_xS_2$ phase, when a Ti^{4+} ($3d^0$) was substituted by an electron-rich Nb^{4+} ($4d^1$), the *c* parameter increased while the *a* parameter decreased, over the range *x* 0 to 0.98 [20]. In the same way, the replacement of tantalum atoms by rhenium atoms in $Ta_{1-x}Re_xSe_2$ phase led to an increase in *c* and a decrease in *a* parameter as the Re/Ta ratio increased [20].

Our work shows that with increased doping there is a decrease in *c* and an increase in *a,* and a decrease of the *c/a* ratio (Table 1). In $MoSe_2$, the charge balance is $Mo^{4+}(Se^{2-})_2$ with molybdenum in oxidation state Mo^{4+} ($4d^2$). Every molybdenum atom should then engage four electrons in the Mo-Se bonds, with the non-bonding Mo $4dz^2$ orbitals holding two electrons per $MoSe_2$ [22]. Niobium (|Kr| $4d^4\ 5s^1$) exists in its compounds in oxidation states: Nb^{3+} ($4d^2$), Nb^{4+} ($4d^1$) and Nb^{5+} ($4d^0$). We showed previously [9] that the insertion of niobium into the network of MSe_2 creates deep donor levels, which then enhance the n-type character of the single crystals obtained with a metallic character that increases with doping. It was suggested that the donor level requirement is that this metal exists in the network of $MoSe_2$ as Nb^{5+}. This means that niobium ions, which can be substituted for molybdenum, should engage four electrons in Mo-Se bonds. The fifth electron is then left out of the network in the donor levels. The replacement of molybdenum atoms by niobium atoms results in fewer electrons in the layers, and consequently fewer electrons in the non-bonding orbitals. The selenium atoms are less repulsed by the non-bonding orbitals. Therefore one has to consider the inner shell repulsion between the selenium atoms in a van der Waals sheet. However, the repulsion of the selenium $3p_x$ and $3p_y$ orbitals within a sheet is stronger than the repulsion of filled $3p_z$ orbitals between sheets. To reduce repulsion of the $3p_x$ and $3p_y$ orbitals, a structural rearrangement takes place to increase the distance along *a* and *b*-directions. The result is an increase in *a* and a decrease in *c* as the Nb/Mo ratio increases.

Doped powders of diselenides $W_{1-x}Nb_xSe_2$

A and B types 1 % niobium-doped WSe_2 samples have the same morphological features as undoped WSe_2. In contrast to the B type 1 % niobium-doped $MoSe_2$ sample, the B type 1 % niobium-doped WSe_2 sample does not show any peculiarity in comparison with the undoped B type WSe_2 sample. The XRD patterns (Figure 8) for both A and B types WSe_2 samples show the same narrow diffraction lines that have already been described for the undoped samples. The refined lattice parameters and the Se/W ratios are listed in Table 1 and Table 2, respectively. Both A and B types crystallize in the WSe_2 hexagonal structure and Table 1 shows that *a* increases and *c* decreases for both A and B types of samples. For the B type WSe_2 sample, we

also observe a gradual decrease in the crystallite size with increasing niobium content (Table 4). The explanations given above regarding the *c/a* ratio and the crystallite size may also be applied here.

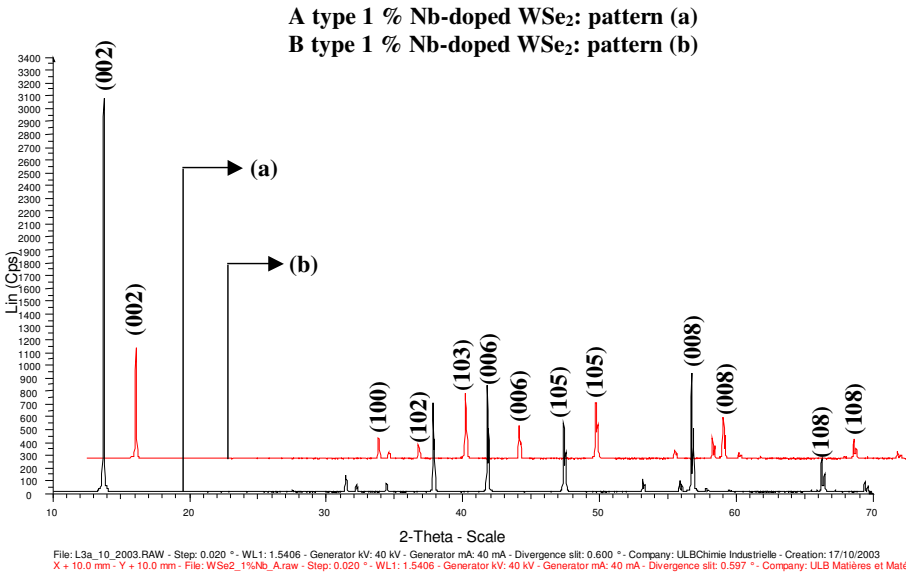

Figure 8. Comparison of X-ray diffraction patterns of A and B type 1 % niobium-doped tungsten diselenide polycrystalline powders: (a) A type 1 % Nb-doped WSe_2: scale (X, Y), (b) B type 1 % Nb-doped WSe_2: scale (X + 10.0 mm, Y + 10.0 mm).

CONCLUSION

(1) Polycrystalline niobium-doped solid solutions, formulated as $M_{1-x}Nb_xSe_2$ (M = Mo, W), were synthesized in silica glass tubes sealed under secondary vacuum. Two procedures have been used for the synthesis: A type samples were obtained at 600 °C and B type samples at 750 °C.

(2) SEM images showed that the A type crystallites of $M_{1-x}Nb_xSe_2$ were larger than the B type. The A type samples gave crystals with more defects on their surfaces, whereas the B type samples were smoother. The B type $Mo_{1-x}Nb_xSe_2$ samples comprised two types of particles. Small particles formed blocks the large particles were hexagonal. Chemical composition analysis showed that the large particles were consistent with a niobium-doped $MoSe_2$ composition while the small ones were Se-poor.

(3) X-ray analysis and chemical composition analysis of the undoped samples showed that a mixed-stacking of $2H_b$-and 3R-type layers could be assumed for B type $MoSe_2$ polycrystalline powders in agreement with previous work published. Only the A type $MoSe_2$ polycrystalline powder showed a genuine $2H_b$-structure. Similar results were obtained for A and B type WSe_2 polycrystalline powders.

(4) X-ray analysis of all $Mo_{1-x}Nb_xSe_2$ and $W_{1-x}Nb_xSe_2$ solid solutions showed that all diffraction patterns agreed with those of the hexagonal values of $MoSe_2$ and WSe_2 respectively, but the B type $Mo_{1-x}Nb_xSe_2$ solid solutions exhibited broader diffraction lines with increasing amounts of niobium suggesting some inhomogeneous distribution of niobium. Moreover these samples showed a gradual decrease of the crystallite size with an increasing niobium concentration

suggesting an increase in defect density. The effects of doping for all niobium-doped samples were an increase in *a* and a decrease in *c*, which led to a decrease of the *c/a* ratio
(5) Single crystals of $MoSe_2$ and WSe_2 have already been obtained from polycrystalline A type powders. Preparation of single crystals from polycrystalline B type powders is under investigation in our laboratory.

ACKNOWLEDGEMENTS

This work was sponsored by the Commission Universitaire pour le Développement (CUD)-Communauté française de Belgique. Their financial support is gratefully acknowledged. Moussa Bougouma and Boubié Guel would like to thank the CUD-CIUF for receiving fellowships to stay at the Université libre de Bruxelles within the framework of the Institutional cooperation project between the Communauté française de Belgique and the University of Ouagadougou. We also thank Dr. J. Dille for helpful discussion on the electron diffraction of the samples.

REFERENCES

1. Vollath, D.; Szabo, D.V. *Acta Mater.* **2000**, 48, 953.
2. Morales, J.; Santos, J.; Tirado, J.L. *Solid State Ionics* **1996**, 83**,** 57.
3. Desphande, M.P.; Patel, P.D.; Vashi, M.N.; Agarwal, M.K. *J. Crystal Growth* **1999**, 197**,** 833.
4. Tributsch, H. *Z. Naturforsch*. **1977**, 32a, 972.
5. Tributsch, H.; Bennet, J.C. *J. Electroanal. Chem. Interface Electrochem*. **1977**, 81, 97.
6. Tributsch, H.; Gerischer, H.; Clement, C.; Buche, E. *Ber. Bunsenges, Physik. Chem*. **1979**, 83, 655.
7. Wilson, J.A.; Yoffe, A.D. *Adv. Phys*. **1969**, 18, 193.
8. Prasad, G.; Srivastana, O.N. *J. Phys. D* **1988**, 21, 1028.
9. Legma, J.B.; Vacquier, G.; Traoré, H.; Casalot, A. *Mat. Sci. Eng*. **1991**, B8, 167.
10. Klein, A.; Dolatzoglou, P.; Lux-Steiner, M.; Bucher, E. *Solar Energy Mater. Solar Cells* **1997**, 46**,** 175.
11. Naruke, H.; Wakatsuki, N.; Hoshi, Y.; Sasaki, Y. *Mat. Res. Bull.* **1996**, 31, 647.
12. Bujewski, A.; Kwiatkowska, I.; Masiakowski, H.; Dobrowolski, J. *Chemia* **1983**, 108**,** 21.
13. *JCPDS X-ray Powder Data file*, Pattern: 01- 077-1715.
14. *JCPDS X-ray Powder Data file*, Pattern: 01- 087-2418.
15. Hayashi, K.; Ikeuchi, T.; Takeuchi, H.; Shimakawa, M. *J. Alloys Comp.* **1995**, 219, 161.
16. Pratap, R.; Gupta, R.K. *Phys. Status Solidi*. **1972**, A 9, 415.
17. Baglio, J.; Kamieniecki, E.; DeCola, N.; Struck, C. *J. Solid State Chem*. **1983**, 49, 166.
18. Gande, T.; Ley, L.; Cardona, M. *Phys. Rev. Let*. **1977**, 38, 872; **1977**, 38, 1033.
19. Sienicki, W. *Mater. Chem. Phys*. **2001**, 68, 119.
20. Furuseth, S. *J. Alloys Comp.* **1992**, 178**,** 211.
21. Celine Sortais-Soulard, *Thesis*, *Ecole Doctorale STIM Nantes*, University of Nantes, France, **2004**.
22. Tributsch, H. *J. Electrochem. Soc*. **1978**, 125, 1086.